The Astrophysical Journal, 686:1155–1161, 2008 October 20

FAR-ULTRAVIOLET OBSERVATIONS OF THE OPHIUCHUS REGION WITH SPEAR

D.-H. Lee,[1,2] K.-I. Seon,[1] K. W. Min,[3] Y. S. Park,[1] I. S. Yuk,[1] J. Edelstein,[4]
E. J. Korpela,[4] R. Sankrit,[4] S. J. Park,[3] and K. S. Ryu[3]
Received 2007 July 1; accepted 2008 July 2

ABSTRACT

We present the first far-ultraviolet (FUV; 1370–1670 Å) image of the Ophiuchus molecular cloud region, observed with the SPEAR imaging spectrograph. The flux levels of the diffuse FUV continuum are in reasonable agreement with those of the *Voyager* observations in the shorter FUV wavelengths (912–1216 Å), provided that the diffuse FUV emission is dominated by the spectra from late O- and early B-type stars. The observed region of the present study was divided into five subregions according to their FUV intensities, and the spectrum was obtained for each subregion with prominent H_2 fluorescent emission lines. A synthetic model of the H_2 fluorescent emission indicates that the molecular cloud has more or less uniform physical parameters over the Ophiuchus region, with a hydrogen density n_H of 500 cm^{-3} and a H_2 column density $N(H_2)$ of 2×10^{20} cm^{-2}. It is notable that the observed diffuse FUV continuum is well reproduced by a single-scattering model with scattered starlight from the dust cloud located at ~120–130 pc, except at a couple of regions with high optical depth. The model also gives reasonable properties of the dust grains of the cloud with an albedo a of 0.36 ± 0.20 and a phase function asymmetry factor g of 0.52 ± 0.22.

Subject headings: ISM: individual (Ophiuchus) — ISM: lines and bands — ultraviolet: ISM

Online material: color figures

1. INTRODUCTION

Far-ultraviolet (FUV) photons are important for the physical and chemical processes in the interstellar medium (ISM) as they ionize atoms, dissociate molecules, and heat gases and dust (see Spitzer 1978). Hence, extensive observations of FUV radiation have been made in order to study molecular hydrogen in the ISM. For example, FUV absorption-line observations by the satellites *Copernicus* (Spitzer & Jenkins 1975; Savage et al. 1977), Hopkins Ultraviolet Telescope (HUT; Gunderson et al. 1998), *Orbiting and Retrievable Far and Extreme Ultraviolet Spectrometer* (*ORFEUS*; Dixon et al. 1998; Ryu et al. 2000; Lee et al. 2000), and the *Far Ultraviolet Spectroscopic Explorer* (*FUSE*; Shull et al. 2000; Tumlinson et al. 2002; Richter et al. 2003) provided valuable information regarding H_2 for selected regions in the Galaxy and the Magellanic Clouds. Recently, the SPEAR (Spectroscopy of Plasma Evolution from Astrophysical Radiation) mission, with its first large-area spectral sky survey of cosmic FUV radiation (Edelstein et al. 2006a, 2006b), enabled the spectral and imaging study of H_2 molecular clouds (Lee et al. 2006, hereafter Lee06), as well as supernova remnants (Seon et al. 2006a; Nishikida et al. 2006) and superbubbles (Ryu et al. 2006; Kregenow et al. 2006).

While most of the diffuse interstellar FUV continuum radiation is believed to be from starlight scattered by interstellar dust (Schiminovich et al. 2001; Bowyer 1991; Lee06), diffuse H_2 fluorescence is also detectable in photodissociation regions (PDRs) where H_2 molecules are electronically excited by absorbing FUV photons in the Lyman and Werner bands (Lee06 and references therein). Therefore, observing both diffuse FUV continuum scattered by interstellar dust and the diffuse H_2 fluorescent emission from interstellar clouds provides an excellent opportunity to study the relationship between the gas and dust components and understand the physical and chemical environment of the clouds. In addition, the diffuse FUV observation may also reveal scattering properties of interstellar dust grains, such as the albedo a and phase function asymmetry factor g.

The Ophiuchus molecular cloud is a well-known birthplace of stars. The "conventional" distance of ~165 pc to the cloud was derived from multicolor photometry of heavily absorbed stars in the ρ Ophiuchus core (Chini 1981). However, a significantly closer distance of ~120–135 pc has been suggested by recent studies based on the photometric distances to members of the Sco-Cen OB association (de Geus et al. 1989) as well as the improved stellar distances obtained with *Hipparcos* parallaxes (Knude & Høg 1998). More recently, Lombardi et al. (2008) combined the extinction maps from the 2MASS with *Hipparcos* parallaxes to obtain the distance of ~120 pc and the thickness of ~28 pc, except for the core region of which the distance was estimated to be ~130 pc. On the other hand, Loinard et al. (2008a, 2008b) report that two objects associated with the Oph A have a distance close to ~120 pc while two others associated with the Oph B have a distance of ~165 pc. Loinard et al. (2008b) and Lombardi et al. (2008) argue that the latter objects may not be directly associated with the Ophiuchus complex. Holberg (1990) discovered diffuse FUV (912–1216 Å) radiation in the region with *Voyager* UVS and interpreted the diffuse emission as starlight scattered by interstellar dust, as in reflection nebulae. Sujatha et al. (2005) reexamined these observations, together with others from the *Voyager* archives and suggested that the diffuse radiation is almost entirely due to the scattering from a foreground dust cloud closer than 160 pc. Three-dimensional distribution of the matter in this region was determined with CO (Dame et al. 2001). Young et al. (2006) surveyed the dust continuum emission of the Ophiuchus molecular cloud with 1.1 mm BOLOCAM and found that the distinct cores comprise 0.5%–2% of the total cloud mass.

In this paper new observations of the Ophiuchus region taken with the FUV imaging spectrograph SPEAR are reported. More

[1] Korea Astronomy and Space Science Institute, Daejeon, Korea, 305-348; kiseon@kasi.re.kr.
[2] California Technology Institute, Pasadena, CA 91125; dhlee@caltech.edu.
[3] Korea Advanced Institude of Science and Technology, Daejeon, Korea 305-701; kwmin@space.kaist.ac.kr, einpark@kasi.re.kr, ksryu@satrec.kaist.ac.kr.
[4] Space Sciences Laboratory, University of California, Berkeley, CA 94720; jerrye@ssl.berkeley.edu, korpela@ssl.berkeley.edu, ravi@ssl.berkeley.edu.

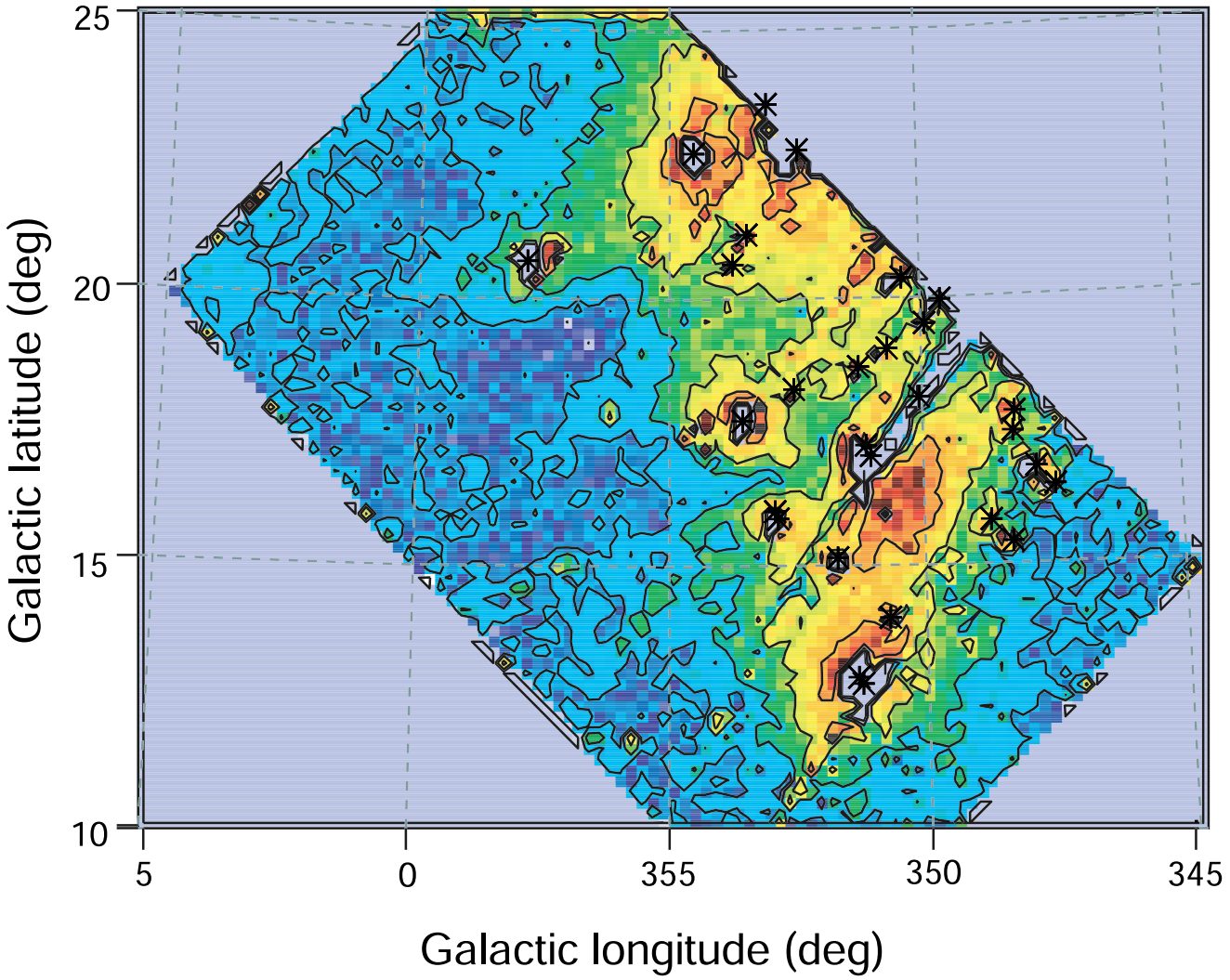

FIG. 1.—FUV (1370–1670 Å) map of the Ophiuchus region obtained from the survey observations by SPEAR. The pixel size is $0.2^\circ \times 0.2^\circ$. The colors represent the FUV intensity: (1) a blue region (0–4000 CU), (2) a sky-blue region (4000–8000 CU), (3) a green region (8000–16,000 CU), (4) a yellow region (16,000–32,000 CU), and (5) a red region (32,000–64,000 CU). The pixels with >64,000 CU, which correspond to the stars and nearby regions, are not included in our analysis. The bright *TD-1* catalog stars ($>1 \times 10^{11}$ ergs cm^{-2} s^{-1} sr^{-1} Å^{-1}) are overplotted in the figure.

specifically, we present the first FUV continuum image ($15^\circ \times 25^\circ$) of the region, which is believed to map the dust-scattered starlight. We compare our results with the IR 100 μm map observed by *IRAS* and the short wavelength FUV (912–1216 Å) observation by *Voyager* UVS. H_2 fluorescent emission spectra of subregions, divided according to their FUV intensities, are also presented along with model estimations of the hydrogen density and the H_2 column density. Finally, we suggest the distance to the cloud and the scattering properties of the dust grains by analyzing the observed FUV map with the result of a single-scattering model in which starlight is predominantly scattered in the forward direction.

2. FAR-ULTRAVIOLET OBSERVATIONS AND ANALYSIS

The SPEAR mission employs an imaging spectrograph with two channels (Short and Long) that is optimized for the observation of diffuse emission lines at FUV wavelengths. Only the Long channel data was utilized for this study. The Long channel covers 1350–1700 Å with a resolving power of $\lambda/\Delta\lambda \sim 550$. The field of view of the Long channel is $7.4^\circ \times 4.3'$ with a 5′–15′ imaging resolution along the slit. The spectral half-energy line width, averaged over the angular field, is 3.2 Å. The instrument, its in-orbit performance, and the data analysis procedures are described in Edelstein et al. (2006a, 2006b). The systematic error in the intensity calibration of the instrument was estimated to be about 25%.

Our data set is composed of 57 scanning observations made during a sky survey toward the Ophiuchus region. The total exposure time is approximately 300 s per pixel. The internal detector background, measured during an observation of 5 s at 25 s intervals by closing the shutter, is 0.01 counts s^{-1} Å^{-1} and is subtracted from the data, resulting in typical residual rates of $\sim$1 counts s^{-1} Å^{-1}. Only the data from 1370 to 1670 Å, excluding the intense O I airglow line at 1356 Å, were used in the present analysis.

Figure 1 shows the observed FUV (1370–1670 Å) continuum map of the Ophiuchus region with Galactic coordinates of a $20^\circ \times 15^\circ$ area with $0.2^\circ \times 0.2^\circ$ pixels. Selected *TD-1* catalog stars ($>1 \times 10^{-11}$ ergs cm^{-2} s^{-1} sr^{-1} Å^{-1}) from Thompson et al. (1978) are marked with asterisks. The spectral type and distance adopted from the *Hipparcos* catalog (Perryman et al. 1997) of each star are presented in Table 1. We divided the map into five distinctive FUV intensity regions represented by colors: (1) a blue region with <4000 photons cm^{-2} s^{-1} sr^{-1} Å^{-1} (hereafter CU), (2) a sky-blue region (4000–8000 CU), (3) a green region

TABLE 1
IDENTIFICATION OF BRIGHT STARS OBSERVED WITH SPEAR

HD	l (deg)	b (deg)	d (pc)	Spectral Type	FUV Flux	$E(B-V)$	τ_{FUV}	Name
146624	348.56	15.41	43.05	A0 V	4.79	0.00	0.02	d Sco
148898	356.30	17.83	53.59	A7 p	4.44	0.00	0.00	V ω Oph
145483	347.74	16.50	91.41	B9 V	5.67	0.06	0.41	SV ZI 1217
150768	353.35	11.88	91.74	A2 V	6.61	0.05	0.36	NSV 7935
145127	350.29	19.51	103.09	A0 V	6.65	0.02	0.13	
145964	353.72	21.16	105.82	B9 V	6.42	0.00	0.00	
151012	354.21	12.12	110.13	B9.5 V	7.03	0.06	0.42	
148562	353.16	15.94	112.36	A2 V	7.81	0.12	0.88	
147779	347.49	12.42	116.28	A0 V	7.14	0.00	0.00	
144661	349.99	19.97	117.65	B8 IV	6.32	0.08	0.56	
148605	353.10	15.80	120.48	B3 V	4.79	0.11	0.83	i Sco
147703	350.64	15.40	120.92	B9 Vn	7.47	0.18	1.28^{core}	
146416	353.98	20.60	125.16	B9 V	6.61	0.05	0.39	
144844	350.73	20.37	130.72	B9 IV	5.86	0.07	0.50	SV ZI 1208
149438	351.53	12.81	131.75	B0 V	2.83	0.08	0.58	τ Sco
147889	352.86	17.04	135.87	B2 III	7.90	0.99	7.20^{core}	
145792	351.01	19.03	138.89	B6 IV	6.42	0.20	1.42^{core}	V V1051 Sco
146001	350.39	18.12	141.64	B8 V	6.06	0.14	1.01^{core}	
145482	348.12	16.84	143.47	B2 V	4.58	0.06	0.43	13 Sco
146606	348.98	15.81	146.84	A0 V	7.08	0.00	0.00	
148184	357.93	20.68	149.93	B2 Vne	4.26	0.45	3.26^{150}	V χ Oph
144925	354.47	23.53	150.60	A0 V	7.79	0.24	1.77^{150}	
148199	349.46	13.48	150.60	B8 Vp	7.01	0.13	0.92	V V1028 Sco
147196	352.80	18.24	151.29	B6 Vn	7.05	0.22	1.59^{core}	
148438	358.60	20.66	156.01	A0 IV	7.17	0.27	1.99^{150}	

NOTE.—The symbols "150" and "core" indicate the stars located in the regions corresponding to $d \sim 150$ pc in Fig. 3*b* and the Ophiuchus core in Fig. 3*a*, respectively. Note that all the FUV optical depths are high ($\tau > 1$).

(8000–16,000 CU), (4) a yellow region (16,000–32,000 CU), and (5) a red region (32,000–64,000 CU). The pixels with > 64,000 CU, that correspond to the stars and their adjacent regions were not included in this analysis.

The present continuum map was verified using the FUV observations made by *Voyager*. Among the 31 positions observed by *Voyager* (Sujatha et al. 2005), the FUV intensities at 11 locations within the area of the current map were compared. Table 2 shows that the ratios between the two FUV wave bands vary from 0.7 to 2.3. If it is assumed that the dominant sources of the diffuse FUV radiation in this region are the stars of spectral type B3 V–O9 V, as shown in Table 2 of Sujatha et al. (2005), the SPEAR results seem to be in accord with the observations of *Voyager* within acceptable levels of uncertainty, as the intensity ratios between the wave bands 912–1216 and 1370–1670 Å of these stars are 0.8–1.5 (Castelli & Kurucz 2003).

TABLE 2
FUV FLUXES OBSERVED BY *Voyager* AND SPEAR

Location[a]	l (deg)	b (deg)	FUV[a] (912–1216 Å) (CU)	FUV[b] (1400–1650 Å) (CU)
1	359.8	17.8	1900 ± 170	2730 ± 680
2	0.2	22.1	2200 ± 140	2000 ± 500
5	0.6	21.4	3200 ± 140	1480 ± 370
6	1.4	19.7	3270 ± 360	3970 ± 990
7	0.4	16.8	3320 ± 140	1980 ± 495
11	2.4	19.2	3740 ± 310	2970 ± 740
12	348.1	12.1	4080 ± 360	2860 ± 715
13	2.4	18.7	4310 ± 65	4610 ± 1150
21	348.5	12.2	5760 ± 445	8600 ± 2150
22	359.2	23.5	5940 ± 95	4590 ± 1150
30	354.3	13	10900 ± 570	4650 ± 1160

[a] The location numbers and the FUV intensities observed by *Voyager* are from Sujatha et al. (2005).
[b] Observed by SPEAR.

3. DISCUSSION

3.1. *FUV Continuum and* H_2 *fluorescence*

When the present FUV map of the Ophiuchus region is compared with the *IRAS* 100 μm map by Sujatha et al. (2005), two main features are readily notable. First, the FUV and IR emissions show relatively weak correlations. For example, the Ophiuchus core region (around $l = 351^\circ$–353°, $b = 16^\circ$) shows a strong emission in both the FUV and IR wavelengths, while in the area northeast of the core region (around $l = 356^\circ$, $b = 22^\circ$) FUV intensity is high but IR emission is weak. Furthermore, FUV emission with more than 2000 CU is seen over the whole region of Ophiuchus, even where the IR emission is very weak. Second, the FUV intensity appears to be correlated with stars, while the *IRAS* 100 μm emission map shows no clear relationship with the stars. The extended FUV halos seen around the stars imply the existence of dust in front of the stars, considering the strong forward-scattering nature of the interstellar dust grains, as will be discussed in § 3.2. Hence, in the present case of the Ophiuchus region, the FUV continuum seems to be correlated more with the in situ interstellar radiation field than with the total column density of the dust.

We obtained the spectra for the five subregions denoted with colors in Figure 1, which are divided according to their intensity levels. As can be seen in Figure 2, each FUV spectrum of subregions 1–4 contains prominent H_2 fluorescent emissions above a continuum level, so we fitted each spectrum from subregions 1–4

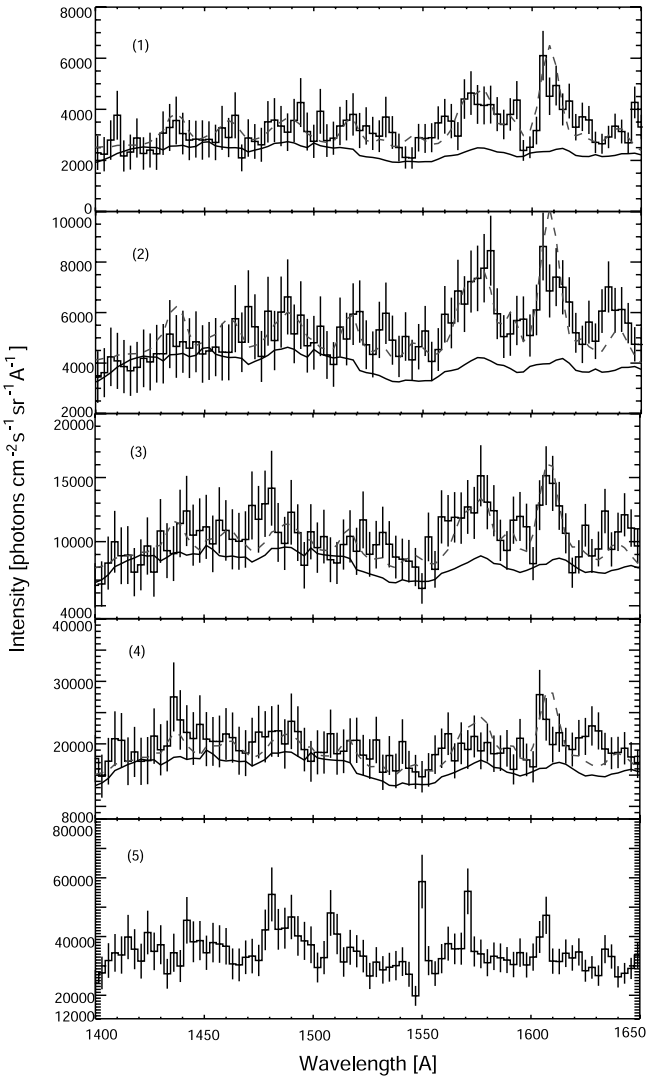

FIG. 2.— FUV spectra (*solid histograms*) of the five subregions defined in Fig. 1 with statistical error bars. We have smoothed the spectra by three bins for better appearance. Spectrum 5 is scaled and smoothed to be used as a background continuum, shown as solid lines in spectra 1, 2, 3, and 4, for fitting CLOUD model (*dashed line*). [*See the electronic edition of the Journal for a color version of this figure*.]

using a H_2 fluorescent emission model and a model continuum. The model continuum was generated by smoothing (over 21 bins) and scaling the spectrum of subregion 5, which is close to the stars, on the basis that dust-scattered light from the stars dominates the continuum spectrum. The peak lines at 1480, 1510, 1550, 1570, and 1605 Å in the spectrum of subregion 5, which are mainly from the stellar atmosphere, are smoothed out in the present analysis. To model the H_2 fluorescent emission lines, CLOUD, a plane parallel H_2 model program for the PDRs, was used. The basic concepts, physical backgrounds, and application of the model are described in Black & van Dishoeck (1987). While many input parameters were required for modeling, only three main parameters are of interest in this study: the enhancement factor of the incident FUV intensity (I_{UV}) compared with the mean interstellar value adopted by Draine (1978), the cloud density n_H, and the total H_2 column density $N(H_2)$. We generated 4800 synthetic models with $n_H = (10,\ 50,\ 100,\ 500)$ cm^{-3}, $N(H_2) = (0.1\text{–}20) \times 10^{20}$ cm^{-2}, and $I_{UV} = (0.01\text{–}3)$ in an effort to determine the best fit to the observed FUV fluorescence. The model parameters of CLOUD and the scale factor of the model continuum were determined by minimizing the χ^2 values. The solid lines and the dashed lines in Figure 2 represent the scaled continuum spectra and the H_2 fluorescent emissions of the best-fit model for subregions 1–4, respectively. Table 3 shows the model parameters and the reduced χ^2 values χ^2_ν, as well as the total FUV intensity, the FUV continuum intensity, and the H_2 fluorescent emission intensity.

The best-fit model parameters in Table 3 show that all of the subregions 1–4 have similar hydrogen density n_H and total H_2 column density $N(H_2)$ values. This constancy indicates that the H_2 fluorescence could originate from a relatively uniform molecular cloud over the Ophiuchus cloud region, which is consistent with the continuum map analysis. The physical parameters of this foreground component are derived as $n_H = 500$ cm^{-3} and $N(H_2) = 2 \times 10^{20}$ cm^{-2}, although systematic variance of nearly 25% exists in the determined $N(H_2)$ value together with approximately 50% for n_H, due to the discrete model grids utilized here. It is interesting to compare the physical parameters obtained in the Ophiuchus region with those of the Taurus region, which are $n_H = 50$ cm^{-3}, $N(H_2) = 0.8 \times 10^{20}$ cm^{-2}, and $I_{UV} = 0.2$, resulting in an H_2 fluorescent intensity $I(H_2)$ of $\sim 0.2 \times 10^3$ CU (Lee06). We note that the optical depths at 1000 Å by the H_2 self-shielding and the dust absorption processes are comparable when the ratio I_{UV}/n_H is of the order of 1 cm^3 whereas line absorption dominates when $I_{UV}/n_H \ll 1$ cm^3 and dust absorption dominates when $I_{UV}/n_H \gg 1$ cm^3 (Black & van Dishoeck 1987). In both the Ophiuchus and Taurus cases, $I_{UV}/n_H \ll 1$ cm^3, implying that line absorption completely dominates the attenuation of the UV radiation and that most of the available photons dissociate and excite H_2. Therefore, $I(H_2)$ is dependent mainly on I_{UV} rather than $N(H_2)$ or n_H (see Lee et al. 2007). This is in good agreement with the present results: the ratio of I_{UV} of the Taurus halo region to that of the Ophiuchus subregion 1 is 0.2, while the same ratio of $I(H_2)$ is 0.22.

In addition, Table 3 shows that the FUV continuum intensity and the H_2 fluorescence increase from subregions 1–4. For the FUV continuum, it is natural to assume that the FUV continuum scattered by dust strengthens near the stars. However, the H_2 fluorescence radiation does not have to increase with the FUV continuum unless it arises from the same source, that is, the

TABLE 3
BEST-FIT MODEL PARAMETERS AND RESULTANT FUV INTENSITIES OF EACH SUBREGION

Subregion	n^a_H (cm^{-3})	$N^a(H_2)$ (cm^{-2})	I^a_{UV}	χ^2_ν	I_{total} ($I_{con} + I_{H_2}$) 10^3 (CU)	I_{H_2}/I_{con}
1.....	500	2×10^{20}	1.0	0.76	3.2 ± 0.8 (2.3 + 0.9)	0.39 ± 0.05
2.....	500	2×10^{20}	1.5	0.51	5.3 ± 1.3 (4.0 + 1.3)	0.33 ± 0.03
3.....	500	2×10^{20}	2.0	0.21	11.7 ± 2.9 (9.8 + 1.9)	0.19 ± 0.02
4.....	500	3×10^{20}	3.0	0.68	18.9 ± 4.7 (16.2 + 2.7)	0.17 ± 0.01

[a] Best fit model parameters.

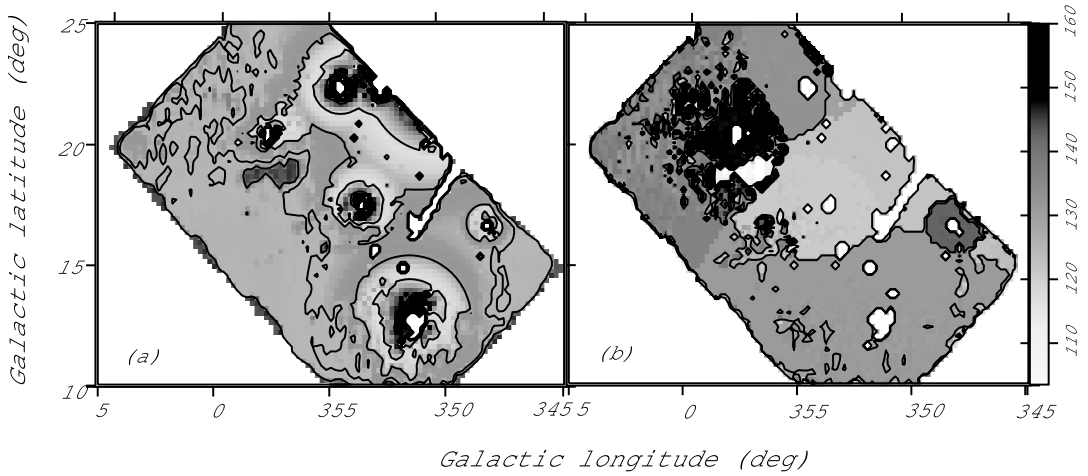

FIG. 3.—(*a*) FUV (1370–1670 Å) intensity map of the Ophiuchus region predicted by the single-scattering model and (*b*) best-fit distance to the scattering layer calculated by the single-scattering model. The color bar indicates the distance value in parsec. [*See the electronic edition of the Journal for a color version of this figure.*]

continuum FUV radiation. The H_2 fluorescence may arise from excited gas at any location along the line of sight up to the opaque molecular cloud surface. Therefore, the correlation seen in the present Ophiuchus cloud may be another indication that the H_2 fluorescence comes from the same foreground cloud layer as the scattered FUV continuum radiation. On the other hand, the FUV continuum intensity in subregion 4 increases nearly sevenfold compared to that of subregion 1, while $I(H_2)$ (or I_{UV}, as explained in the previous paragraph) shows only a threefold increase. This would imply the existence of other sources of the FUV continuum or a more complex cloud structure in subregion 4. It is shown in the next section that the ρ Ophiuchus core located in subregion 4 is optically thick and exhibits distinctively different scattering properties from other subregions.

3.2. *Radiative Transfer Model of Dust Scattering*

The halos around the stars in the FUV map significantly extend beyond the size of instrumental point-spread function, which is at most $\sim 15'$ (Seon et al. 2004), implying their scattering origin. We therefore modeled the diffuse FUV emission from the Ophiuchus cloud complex with a single-scattering model of dust in a manner similar to that used by Shalima & Murthy (2004) and Sujatha et al. (2005). Sujatha et al. (2005) assumed that the distance to the Ophiuchus complex is $\sim$160 pc and that the foreground clouds covering the entire region of the Coalsack and Chamaeleon-Musca clouds (Corradi et al. 2004) continue into the Ophiuchus area. From their model, Sujatha et al. (2005) concluded that the diffuse FUV radiation is attributable to scattering in one of these foreground clouds. Based on the recent estimates of the distance to the Ophiuchus complex, $\sim$120–135 pc; however, the foreground cloud assumed by Sujatha et al. (2005) would be in fact the Ophiuchus cloud complex itself. Hence, we have assumed two different geometrical configurations in our model: one is the same as that of Sujatha et al. (2005) with an optically thick cloud at 160 pc and a scattering dust layer in front of the thick cloud, and in the other geometry we considered only a dust-scattering layer without a thick cloud at 160 pc. Our model result showed that the back-scattered light from the optically thick cloud at 160 pc in the first model was an order of magnitude smaller than the forward-scattered component from the closer dust layer. In fact, the result was indistinguishable from that of the second model with the diffuse isotropic FUV background of $\sim$300 CU (Bowyer 1991), of which 144–195 CU is known to be the extragalactic background radiation coming from resolved objects (Gardner et al. 2000), added in the second model. Both of the effects of the optically thick cloud at 160 pc and the extragalactic isotropic FUV background were within the instrumental systematic error rate of 25%.

All stars located at a distance up to 300 pc in the *Hipparcos* catalog were included in the calculation, while only a few of the bright stars are shown in Table 1. Based on the spectral type of each star, a temperature and an effective gravity were derived using the tables from Straižys & Kuriliene (1981), and the spectral energy distribution of the star was calculated by interpolating the grid of the Kurucz model (Castelli & Kurucz 2003). The intrinsic FUV luminosity of the star was obtained by scaling the model flux to the observed V magnitude, and the FUV extinction correction derived from the color excess $E(B-V)$. $E(B-V)$ values and the optical depths in the FUV wavelength are also shown in Table 1.

We varied the distance of the foreground scattering cloud in the 50–160 pc range in both geometries. We found significantly broad profiles in the predicted brightness distributions around some bright stars due to back-scattering when the stars were located in front of the scattering layer, as noted by Witt & Oshel (1977). In this case, not only the brightness distributions, but also the FUV intensities around the stars did not fit the observed values. On the other hand, when the scattering layer is too close to us, bright halos were seen around some nearby stars which did not fit our data. Hence, our model evaluates the FUV emission intensity for each sight line to estimate the distance d of the scattering dust layer with a combination of optical constants a and g that gives the best-fit value to the observed FUV intensity. The optical constants are assumed to have single values throughout the region. The albedo a is determined by the overall absolute values of the diffuse FUV intensity, while the asymmetry factor g is determined by the spatial extents of the dust-scattered halos around the stars. The brightness distribution around a single star could be achieved with several combinations of a, g, d in a single-scattering model. For example, a set of small a, large g, small d and a set of large a, small g, large d could produce a similar dust-scattered halo profile around a star. However, this degeneracy is removed when more than two stars located at different distances contribute to the scattered radiation of the same sight line. Indeed, we found that the halo around a star could not be reproduced when the scattered light from nearby bright stars were not taken into

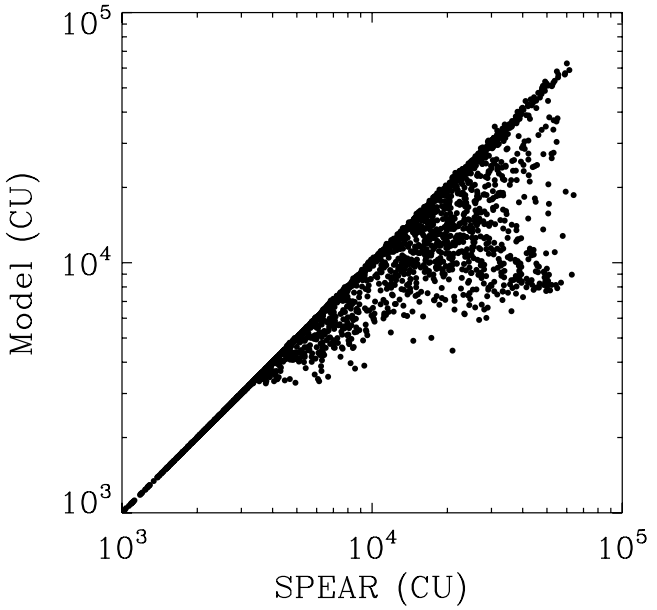

FIG. 4.—Model FUV intensities vs. the observed values.

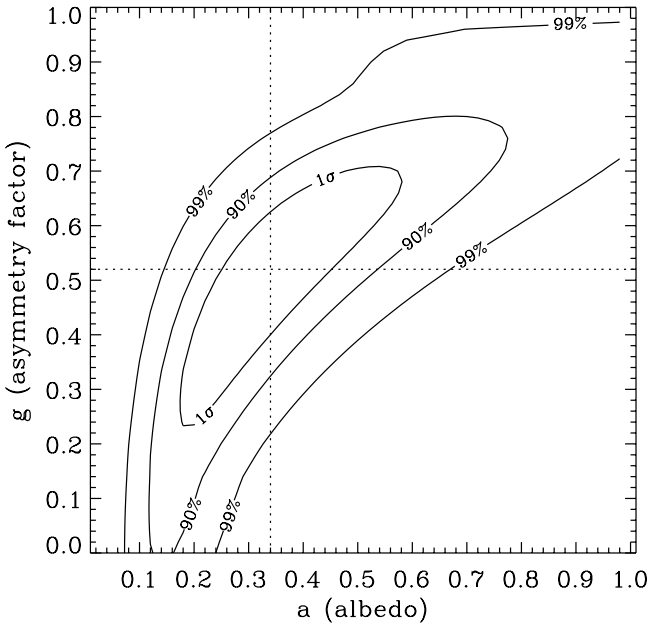

FIG. 5.—Plot of contours of albedo a and asymmetry factor g for the observed Ophiuchus region based on the single-scattering model. The 1 σ confidence contour corresponds to a limit of 0.36 ± 0.20 and 0.52 ± 0.22 on a and g, respectively.

account. The degeneracy of the case with small optical depth τ, large a and that with large τ, small a can also be removed if the degeneracies of a, g, and d were removed. We convolved the predicted brightness distribution with the instrumental point-spread function, although the convolution did not significantly alter the result since the dust-scattering halo was larger than the point-spread function. It should also be noted that the instrumental systematic error rate of 25% dominates the errors of the best-fit parameters.

Although our single-scattering model is rather crude, the result matches the observation very well except for the bright Ophiuchus core region of $(l, b) \sim (352^\circ, 16^\circ)$ in the FUV intensity map (Fig. 3*a*), and for the region of $(l, b) \sim (357^\circ, 20^\circ)$ in the best-fit distance map (Fig. 3*b*). In fact, most of the scattered points in Figure 4 come from the pixels of the core region where our model result predicts lower intensity. Loinard et al. (2008b) and Lombardi et al. (2008) argue that this star-forming core region, corresponding to the Oph B, whose distance was estimated to be ~165 pc by Loinard et al. (2008b), may not be directly associated with the Ophiuchus complex. Hence, the failure of the present model in the core region could be associated with the fact that this star-forming region, located along the line of sight toward the Ophiuchus core and unrelated to the Ophiuchus complex, causes difficulty in interpreting the diffuse FUV radiation from this region. In addition, the high optical depth of the core region could be another source of the error since the present single-scattering model could not adequately describe such a region. Indeed, the best-fit distances in Figure 3*b* show a variation of ~120–130 pc, consistent with the recently estimated distance to the Ophiuchus cloud, except in the region around $(l, b) \sim (357^\circ, 20^\circ)$, where the distance of ~150 pc was found. The inconsistent estimation of the distance around $(l, b) \sim (357^\circ, 20^\circ)$ could also stem from high optical depth of the region, for which multiple-scattering effects should be important. In Table 1 we indicated "150" and "core" for the regions corresponding to $d \sim 150$ pc and the Ophiuchus core, respectively. In both regions, the optical depths are relatively high ($\tau > 1$), implying that multiple-scattering may not be ignored. A more realistic multiple-scattering model would result in a smaller d because of the broadening effect of the scattering halo in the present model. We may, therefore, conclude that the distance to the region around $(l, b) \sim (357^\circ, 20^\circ)$ would be actually closer than 150 pc.

We have derived several contours for a and g in Figure 5. The 1 σ contour corresponds to a limit of 0.36 ± 0.20 and 0.52 ± 0.22 on a and g, respectively. Here, the error range does not take into account the systematic instrumental error. Weingartner & Draine (2001) obtained a slightly higher values of $a = 0.39$ and $g = 0.66$ in the FUV wavelength with an interstellar dust composition model, which are in good agreement with the present result. Multiple-scattering with a higher value of g may yield a dust-scattered halo which is identical in size to that given by single-scattering. In contrast, the albedo a may not change significantly in the multiple-scattering model (especially at the optically thin regions), as at most a factor of a^2 (~13%), which is smaller than the systematic error, is added to the total-scattered light. The geometrical dilution and dust-absorption effects between multiple-scatterings would lower this correction even more. However, the estimate for multiple scattering contribution would not be valid at the optically thick ($\tau > 1$) regions not only because of the significant contribution of multiple scattering but also the high extinction of the scattered light. We have developed a multiple-scattering radiative transfer model to model the global features of the diffuse FUV radiation of our Galaxy (Seon et al. 2006b), and found that the predicted FUV continuum is almost linearly proportional to the albedo a, implying somewhat smaller correction in the multiple-scattering model, because the multiple-scattered radiation coming from optically thick regions is mostly obscured.

In summary, we showed that the overall FUV continuum emission in the Ophiuchus complex is scattered light from the dust layer, which is most likely located at ~120–130 pc. The layer is more or less uniform over the entire region, with a hydrogen density $n_{\rm H}$ of 500 cm^{-3} and the H_2 column density $N(H_2)$ of 2×10^{20} cm^{-2}. The single-scattering model describes the observed features quite well except the core region and the region around $(l, b) \sim (357^\circ, 20^\circ)$, for which multiple-scattering analysis seems necessary. The model also predicts reasonable properties of the

dust grains of the cloud with an albedo a of 0.36 ± 0.20 and a phase function asymmetry factor g of 0.52 ± 0.22.

The authors would like to thank the anonymous referee for the useful comments which helped to clarify and significantly improve the paper. This publication makes use of data products from SPEAR/FIMS, which is a joint project of the Korea Astronomy and Space Science Institute, the Korea Advanced Institute of Science and Technology, and the University of California at Berkeley, funded by the Ministry of Science and Technology (Korea) and by a grant from NASA.

REFERENCES

Black, J. H., & van Dishoeck, E. F. 1987, ApJ, 322, 412
Bowyer, S. 1991, ARA&A, 29, 59
Castelli, F., & Kurucz, R. L. 2003, in IAU Symp., Modelling of Stellar Atmospheres, ed. N. Piskunov, W. W. Weiss, & D.F. Gray (San Francisco: ASP), 20
Chini, R. 1981, A&A, 99, 346
Corradi, W. J. B., Franco, G. A. P., & Knude, J. 2004, MNRAS, 347, 1065
Dame, T. M., Hartmann, D., & Thaddeus, P. 2001, ApJ, 547, 792
Gardner, J. P., Brown, T. M., & Ferguson, H. C. 2000, ApJ, 542, L79
de Geus, de Zeeuw, P. T., & Lub, J. 1989, A&A, 216, 44
Dixon, W. V., Hurwitz, M., & Bowyer, S. 1998, ApJ, 492, 569
Draine, B. T. 1978, ApJS, 36, 595
Edelstein, J., et al. 2006a, ApJ, 644, L153
———. 2006b, ApJ, 644, L159
Gunderson, K. S., Clayton, G. C., & Green, J. C. 1998, PASP, 110, 60
Holberg, J. B. 1990, in IAU Symp. 139, The Galactic and Extragalactic Background Radiation, ed. S. C. Bowyer & C. Leinert, (Dordrecht: Kluwer), 220
Knude, J., & Høg, E. 1998, A&A, 338, 897
Kregenow, J., et al. 2006, ApJ, 644, L167
Lee, D.-H., Min, K. W., Dixon, W. V., Hurwitz, M., Ryu, K. S., Seon, K. I., & Edelstein, J. 2000, ApJ, 545, 885
Lee, D.-H., Pak, S., Dixon, W. V. D., & van Dishoeck, E. F. 2007, ApJ, 655, 940
Lee, D.-H., et al. 2006, ApJ, 644, L181 (Lee06)
Loinard, L., Torres, R. M., Mioduszewski, A. J., & Rodríguez, L. F. 2008a, ApJ, 675, L29
———. 2008b, IAU Symp. 248, A Giant Step: From Milli- to Microarcsecond Astronmetry, ed. W.-J. Jin., I. Platais, & M. A. C. Perryman (Cambridge: Cambridge Univ. Press), 186
Lombardi, M., Lada, C. J., & Alves, J. 2008, A&A, 480, 785
Nishikida, K., et al. 2006, ApJ, 644, L171
Perryman, M. A. C., et al. 1997, A&A, 323, L49
Richter, P., Wakker, B. P., Savage, B. D., & Sembach, K. R. 2003, ApJ, 586, 230
Ryu, K. S., et al. 2000, ApJ, 529, 251
———. 2006, ApJ, 644, L185
Shalima, P., & Murthy, J. 2004, MNRAS, 352, 1319
Savage, B. D., Bohlin, R. C., Drake, J. F., & Budich, W. 1977, ApJ, 216, 291
Schiminovich, D., Friedman, P. G., Martin, C., & Morrissey, P. F. 2001, ApJ, 563, L161
Seon, K.-I., et al. 2004, J. Astron. Space Sci., 21, 399
Seon, K.-I., et al. 2006a, ApJ, 644, L175
———. 2006b, BAAS, 38, 920
Shull, J. M., et al. 2000, ApJ, 538, L73
Spitzer, L. 1978, Physical Processes in the Interstellar Medium (New York: Wiley)
Spitzer, L., & Jenkins, E. B. 1975, ARA&A, 13, 133
Straižys, V., & Kuriliene, G. 1981, Ap&SS, 80, 353
Sujatha, N. V., Shalima, P., Murthy, J., & Henry, R. C. 2005, ApJ, 633, 257
Thompson, G. I., Nandy, K., Jamar, C., Monfils, A., Houziaux, L., Cranochan, D. J., & Wilson, R. 1978, Catalogue of Stellar Ultraviolet Fluxes (London: Sci. Res. Council)
Tumlinson, J., et al. 2002, ApJ, 566, 857
Weingartner, J. C., & Draine, B. T. 2001, ApJ, 548, 296
Witt, A. N., & Oshel, E. R. 1977, ApJS, 35, 31
Young, K. E., et al. 2006, ApJ, 644, 326